Article

Not peer-reviewed version

Polyphenolic Compounds Nanostructurated with Gold Nanopar-Ticles (AuNP-BP) Enhance Wound Repair

Adriana Martínez-Cuazitl , María del Consuelo Gómez-García , Marlon Rojas-López , Raúl Jacobo Delgado-Macuil , Juan Ocampo-López , Gustavo Jesus Vazquez-Zapien , Mónica Maribel Mata-Miranda , David Guillermo Pérez-Ishiwara *

Posted Date: 23 October 2023

doi: 10.20944/preprints202310.1416.v1

Keywords: Polyphenolic-gold nanoparticles conjugates; wound healing model; FTIR analyses of wound repair tissue

Article

Polyphenolic compounds nanostructurated with gold nanopar-ticles (AuNP-BP) enhance wound repair

Adriana Martínez-Cuazitl [1,2], María del Consuelo Gómez-García [1], Marlon Rojas-López[3], Raúl Jacobo Delgado-Macuil [3], Juan Ocampo-López [4], Gustavo Jesús Vázquez-Zapién[5], Mónica Maribel Mata-Miranda[2], and David Guillermo Pérez-Ishiwara [1,*]

[1] Laboratorio de Biomedicina Molecular, ENMyH, Instituto Politécnico Nacional, Mexico City, 07320, Mexico; admartinezc@ipn.mx (A.M.-C.); consuelogg22@yahoo.com.mx (M.C.G.-G

[2] Escuela Militar de Medicina, Centro Militar de Ciencias de la Salud, UDEFA-SEDENA, Mexico City 11200, Mexico; mmcmaribel@gmail.com (M.M.M-M).

[3] Centro de Investigación en Biotecnología Aplicada, Instituto Politécnico Nacional, Tlaxcala, 90700, Mexico; marlonrl1@hotmail.com (M.R.-L.); rdmacuil@yahoo.com.mx (R.J.D.-M.)

[4] Laboratorio de Histología e Histopatología, Universidad Autónoma del Estado de Hidalgo, Hidalgo, 42090, Mexico; jocampo@uaeh.edu.mx (J.O.-L.)

[5] Centro de Investigación y Desarrollo del Ejército y Fuerza Aérea Mexicanos de la Secretaría de la Defensa Nacional (CIDEFAM – SEDENA), Mexico City, 11400, Mexico; gus1202@hotmail.com (G.J.V-Z)

* Correspondence: dperez@ipn.mx, ishiwaramx@yahoo.com.mx; Tel.: +01-55-5538993877, 07320 (D.G.P.-I.)

Abstract: Gold nanoparticles (AuNPs) have been used in a broad range of applications conferring to bio-molecules diverse proprieties such as deliver, stabilization and reduction of adverse effects of drugs or plant ex-tracts. Polyphenolic compounds from Bacopa procumbens (BP) are able to modulate proliferation, adhesion, migration and cell differentiation, reducing artificial scratch area in fibroblast cultures and promoting wound healing in *in vivo* model. Here, chemically synthetized AuNPs conjugated with BP (AuNP-BP) were characterized by Uv-Vis, ATR-FTIR, DLS and zeta-potential. Results showed over-lapping FTIR spectra of polyphenolic compounds from *B. procumbens* capping the AuNPs, stable size by the DLS and zeta potential, AuNP-BP was 44.58 nm, the zeta-potential of AuNPs was -36.3±12.3 mV after conjugation with the BP; - (AuNP-BP), the zeta-potential was reduced to -18-2±7.02 mV. Enhancement of wound healing effect were evaluated by morphometric, histochemical and FTIR changes in rat wound excision model. Results showed that the nanoconjugation process reduced 100 folds BP concentrations to have the same wound healing effect of BP alone. Besides histological and FTIR spectroscopy analyses, demonstrated that AuNP-BP treatment displayed better macroscopical performance; the reduction on inflammatory cells, and the increased synthesis and better organization of collagen fibers.

Keywords: polyphenolic-gold nanoparticles conjugates; wound healing model; FTIR analyses of wound repair tissue

1. Introduction

Wound healing is a complex and coordinated process that involves different kind of cells and molecular signaling. The main objective of this process is to restore physiological and esthetical proprieties. The last step involves the collagen type III substitution by collagen type I and the reordered of both type of fibers to improve the mechanical proprieties. Injures remain as a clinical problem due early and late complications, otherwise the incidence of chronic wounds has rapidly increased due to the rising prevalence of type 2 diabetes, peripheral vascular disease, and metabolic syndrome [1–3].

Even though, fast and optimal wound closure are the main aims for wound care, no topically effective medication has been developed to accelerate the wound healing process and/or to prevent abnormal wound healing [4].

 doi:10.20944/preprints202310.1416.v1

Wound healing effects of phenolic compounds such as flavonoids, secoriridoids, phenolic acids, phenolic alcohols and lignans have been studied, due their antioxidant, antimicrobial, and/or bio-stimulatory properties related to tissue regeneration [5].

Bacopa procumbens has been used in traditional medicine to skin wound healing, their polyphenolic compounds (BP) regulated proliferation and cell adhesion; and enhanced migration in *in vitro* assays; in rat model BP accelerates wound healing process at least 48 h, reducing inflammation, increasing cell proliferation, promoting the deposition and organization of collagen by regulating the canonical and no canonical TGF-β1 expression pathways [6].

Nanoformulation has been successful in transporting, protecting, and delivering active drugs, to obtain synergistic and/or enhanced response at the bio-interface [4,7]. Particularly, due to their unique physical chemical properties, and biocompatibility, gold nanoparticles (AuNPs) have been used in a broad range of applications comprising genomics, biosensors, immune-analysis, clinical chemistry, diagnosis, and pharmaceutics, conferring to biomolecules diverse proprieties such as deliver, stabilization and reduction of adverse effects of drugs or plant extracts [8].

AuNPs could be synthesized by the Au (III) reduction through a simple and reproducible method proposed by Turkevich, using citrate reduction [9].

Surface plasmon resonance (SPR) phenomenon characterized by a strong absorption band in the visible range by the interaction of the light with the unbound balance electrons of the gold, and the other physical and chemical proprieties of AuNPs has been widely characterized by TEM; SEM; Energy Dispersive X ray spectroscopy (EDX); AFM analysis; X ray diffraction (XRD); UV-vis and Fourier Transformed Infrared (FTIR) spectroscopies; Ramman-spectroscopy; and Electrophoretic Ligth Scattering (ELS)[10].

Here, to evaluate the effect of AuNPs in enhancing the bioactive of *B. procumbens* effect in tissue repair of skin injuries, and due biocompatibility and extensive investigation of AuNPs [11,12], we performed the synthesis and characterization of gold nanoparticles functionalized with polyphenolic compounds from *B. procumbens* (AuNPs-BP); subsequently this colloidal dispersion was mixed into a hydrogel for topical administration in the rat excision wound model.

2. Results

2.1. UV–visible spectrophotometry analyses of nanofunctionalized gold nanoparticles with polyphenolic compounds of B. procumbens (AuNP-BP)

The synthesis of gold nanoparticles (AuNP) was performed by the modified Turkevich method, and the red color on the colloid was obtained. Different concentrations of the polyphenolic compounds from *B. procumbens* were conjugated as described in the methodology, the conjugation process changed the red color to brown; the brown color intensity increased proportionally to the BP concentration. To determinate the adequate concentration of the extract that covers the surface of AuNPs, the conjugations (AuNP-BP) were characterized by Uv-visible spectrophotometry.

The UV–visible absorption spectra of AuNPs and AuNP-BP using several concentrations of BP (0.4, 0.8, 1.6, 3.2 and 6.4 mg/ml) are shown in the Figure 1. Single AuNPs showed an intense band centered at 520 nm which is associated to the surface plasmon resonance (SPR). The SPR band of AuNP-BP presented a 4 nm small spectral shift to low energies with respect to AuNPs. At higher concentrations of BP, the AuNP-BP showed an intense band at 668 nm which arises from chlorophyll α [13]; however, the conjugate at 1.6 mg/ml of BP concentration showed the higher intensity of the SPR band without the chlorophyll α peak at 668 nm. Thus, this concentration of BP in the conjugate AuNP-BP was choice to be used in the in vivo healing model; the shape was 28 nm at 2.89846×10^{11} AuNP-BP/ml.

Preprints (www.preprints.org) | NOT PEER-REVIEWED | Posted: 23 October 2023 doi:10.20944/preprints202310.1416.v1

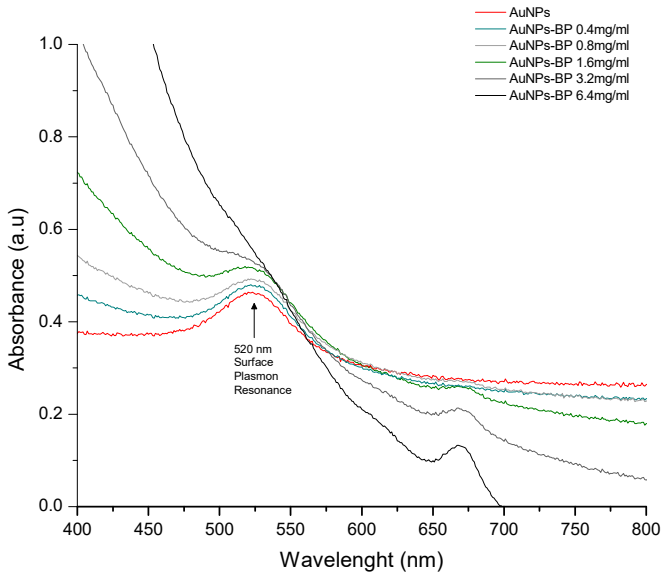

Figure 1. Uv-visible spectra of AuNPs, and the conjugate AuNP-BP at different concentrations of the polyphenolic compounds (BP) from B. procumbens (0.4 - 6.4 mg/mL).

2.1.1. FTIR spectroscopy of the AuNP-BP

AuNPs, BP and conjugate AuNP-BP at 1.6 mg/ml were analyzed by infrared spectroscopy in the fingerprint region (4000-400 cm $^{-1}$) (Figure 2).

A high similarity between the FTIR spectra from both BP and AuNP-BP 1.6 mg/ml was observed. Such similarity is due the AuNPs are conjugated with by molecules of the extract, whereas the AuNPs alone only have citrate groups on their surface, which were formed by the synthesis process.

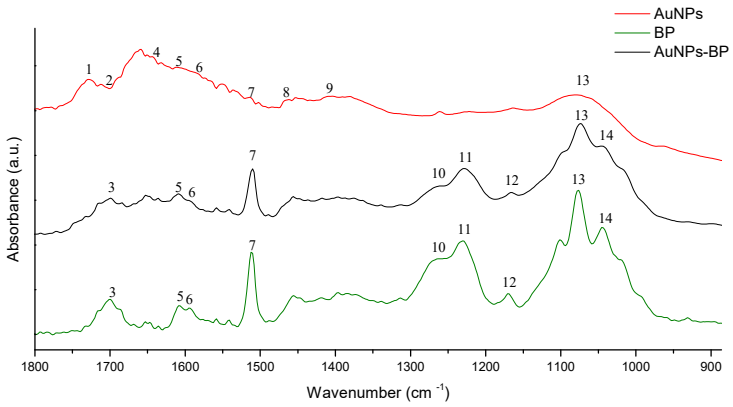

Figure 2. FTIR spectra of AuNPs, BP, and AuNP-BP at 1.6 mg/ml. Band frequencies marked as 1 to 14 are described in Table 1.

Table 1 show band frequencies and functional groups corresponding to the FTIR spectra of AuNPs, BP extract, and AuNP-BP at 1.6 mg/ml. The bands at 1710 cm^{-1}, 1637 cm^{-1}, 1589 cm^{-1}, 1470 cm^{-1}, 1402 cm^{-1} observed in AuNPs are related to N-H and C-O, N-H, CH_2-O, C-C, C=O vibrations from the citrate functional group, respectively [14,15]. In the FTIR spectra of both, AuNP-BP and BP, several bands related directly with the BP chemical compounds were observed. Band at 1700 is related to C=O ester bond; at 1610 is the aromatic double bond; the bands at 1512 cm^{-1} is related to C-O aromatic bond of phenolic compound; the 1450 band is related to aromatic C-C bond; band of 1375 is related to O-H bending,[16] 1258 cm^{-1} and 1230 cm^{-1} arise for C-O on polyols, 1171 cm^{-1}, 1076 cm^{-1}, 1045 cm^{-1}

 doi:10.20944/preprints202310.1416.v1

arisen from C-O from carbohydrates or primary, secondary and tertiary alcohols, respectively, in the BP extract [17]

Table 1. FTIR band frequencies and the related functional groups observed in gold nanoparticles (AuNPs), BP and AuNP-BP conjugate.

Band	AuNPs	BP	AuNP-BP 1.6 mg/ml	Functional group	Reference
1	1742	-	-	O-H on AuNPs	[14]
2	1712	-	-	N-H on AuNPs	[14]
3	-	1703	1703	C=O	[16]
4	1637	-	-	N-H on AuNPs	[15]
5	1612	1608	1608	aromatic double bond	[16]
6	1589	1589	1589	CH2-O on AuNPs	[15]
7	1512	1512	1510	C-C flavonoids and aromatic rings	[17]
8	1470	-	-	C-C on AuNPs	[14]
9	1402	-	-	C=O on AuNPs	[15]
10	-	1258	1259	C-O on polyols	[17]
11	-	1230	1229	C-O on polyols	[17]
12		1171	1165	C-O and –OH of primary alcohols	[17]
13	1076	1076	1074	C-O alcohols, phenols, carboxylic anions	[14,17]
14	-	1045	1055	C-O and –OH of tertiary alcohols	[17]

2.1.2. Dynamic Light Scattering measurements (DLS) and Electrophoretic Ligth Scattering (ELS)

Particle size in their dispersed state in water and the stability of the colloidal system converted to zeta potential were determined. DLS measurement showed that AuNPs size was 44.51 nm while the AuNP-BP was 44.58 nm. The zeta-potential of AuNPs was -36.3±12.3 mV, after conjugation with the BP; - (AuNP-BP), the zeta-potential was reduced to -18-2±7.02 mV (Figure 3).

Preprints (www.preprints.org) | NOT PEER-REVIEWED | Posted: 23 October 2023 doi:10.20944/preprints202310.1416.v1

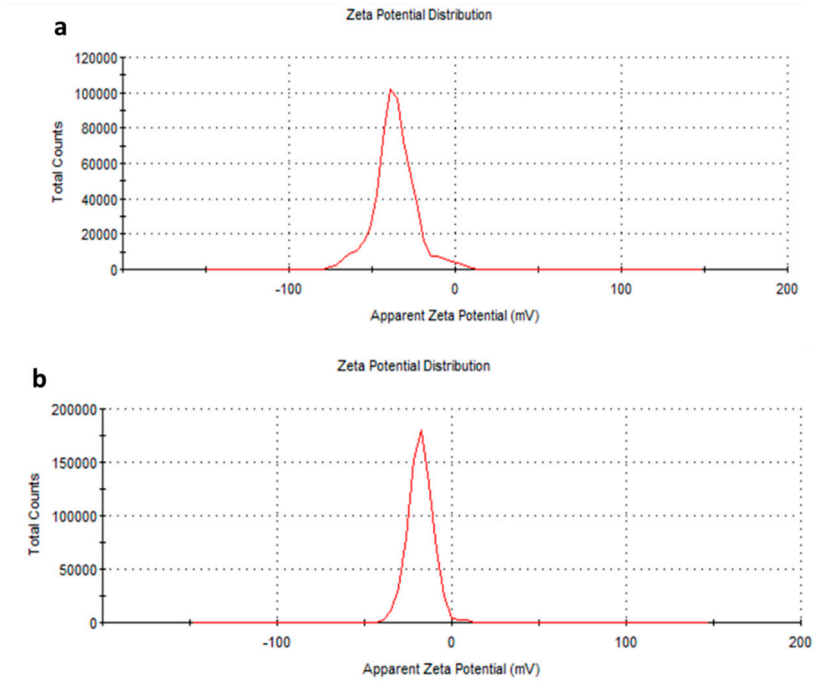

Figure 3. Z potential of (a) AuNPs and (b) AuNP-BP at 1.6 mg/ml.

2.2. Effects of topical application of AuNP-BP hydrogel in rat wound healing model

2.2.1. Macroscopic changes induced by AuNP-BP hydrogel

Macroscopic analysis of wound healing showed improved wound reduction using topical hydrogel with BP or with AuNP-BP hydrogel in comparison to the control group without treatment or to the group treated only with AuNPs. On day 0, the size of wounds in all groups were statistically similar (data not showed). At day 7, wounds treated with BP or AuNP-BP hydrogels presented a moderate scab, while in the group without treatment (WOT) or those animals treated with AuNPs alone, the scab was prominent (Figure 4a). At this time, the reduction of wound area was significantly in the BP and in AuNP-BP hydrogel groups, reducing it in approximately 85% compared to WOT and AuNP groups in which the wound area was reduced only 67% and 73 %, respectively (Figure 4b).

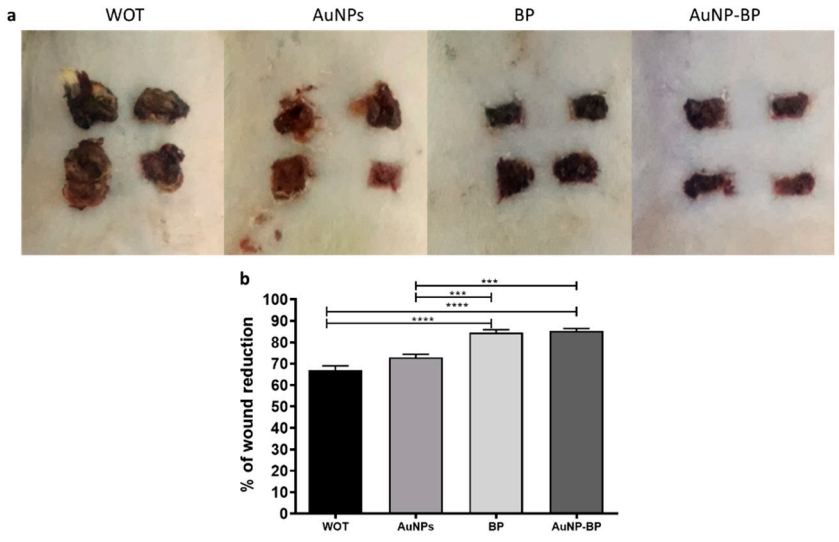

Figure 4. Morphometric changes induced by the different topical treatments. a. Macroscopical changes in groups at 7 days post wound healing. b. Wound reduction area between groups. ***

Preprints (www.preprints.org) | NOT PEER-REVIEWED | Posted: 23 October 2023 doi:10.20944/preprints202310.1416.v1

p<0.001 and **** p <0.0001. WOT, without treatment group; AuNPs, gold nanoparticles group; BP, *B. procumbes* polyphenolic compounds; AuNP-BP, gold nanoparticles conjugated with BP.

2.2.2. AuNP-BP hydrogel enhance histological wound healing

Histopathological analyses of healings at day 7 from injured animal groups without treatment or treated with AuNPs showed an important inflammatory infiltration predominantly of neutrophil cells and few fibroblasts; few blood vessels close to epidermis region were evident and non-re-epithelized tissue was found. Instead, healings from groups treated with BP or with AuNP-BP hydrogels, showed less inflammation and a high number of fibroblasts; interestingly, the injuries presented more blood vessel in dermis and an important re-epitelization process was evident, even thought it was still thin having few stratus (Figure 5).

Masson staining of WOT and AuNP showed some disorganized fibroblasts and an incipient formation of collagen fibers; however, PB and AuNP-BP groups displayed an important quantity of elongated fibroblasts and a better distribution and organization of collagen fibers (Figure 5).

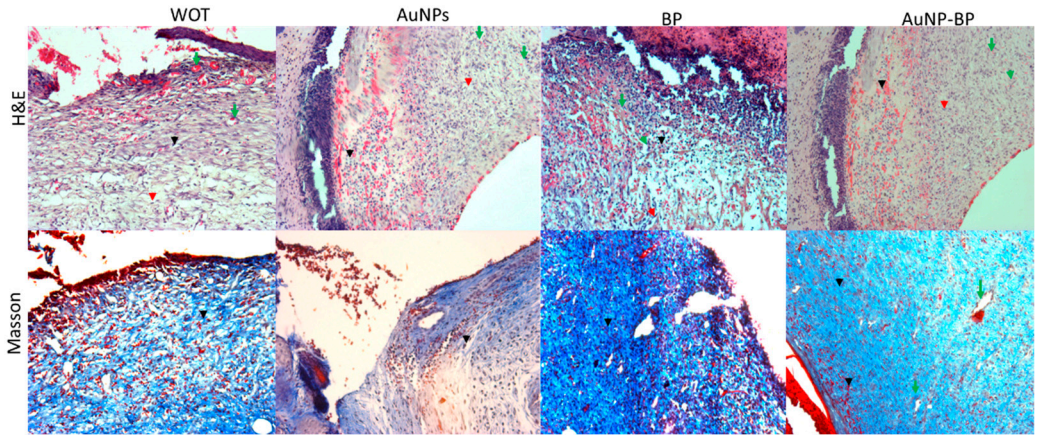

Figure 5. Histological changes of wounds after 7 days of treatments. Representative microphotographs of wounds stained with hematoxylin/eosin (H&E) and Masson's trichrome in WOT, AuNPs, BP, and AuNP-BP. Inflammatory cells (black arrow); fibroblasts (red arrow); blood vessels (green arrow).

Figure 6 showed that wounds from WOT group presented slight, thin and disorganized green fibers (collagen type III) while wounds treated with BP and AuNP-BP hydrogels showed thick and organized red-yellow fibers (collagen type I).

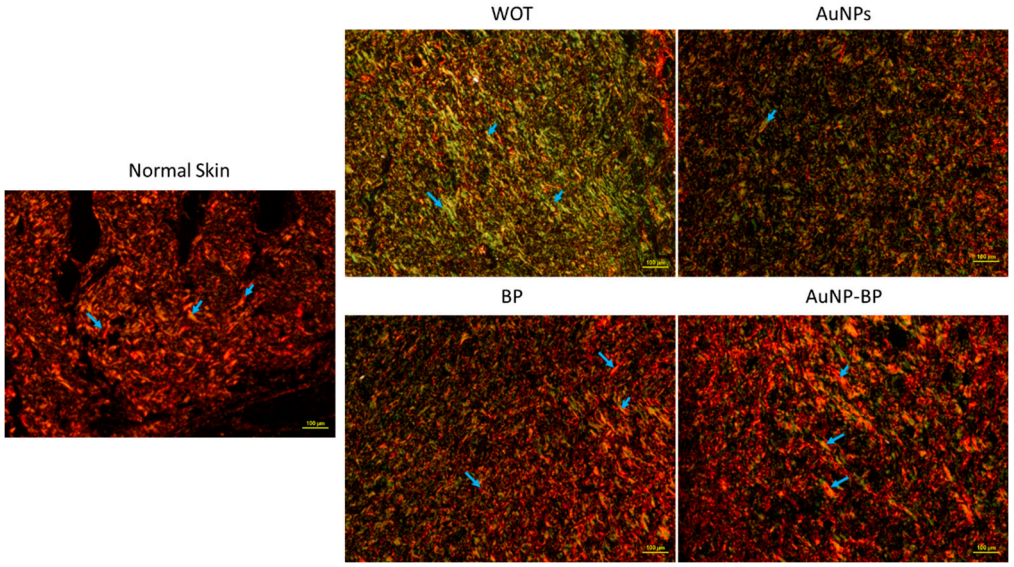

Preprints (www.preprints.org) | NOT PEER-REVIEWED | Posted: 23 October 2023 doi:10.20944/preprints202310.1416.v1

Figure 6. Collagen organization on wounds after 7 days of treatments. Representative microphotographs of Picrosirius Red staining under polarized light in normal skin, WOT, AuNPs, BP, and AuNP-BP. Greenish fibers (collagen type III) and yellow-red fibers (collagen type I). Collagen fibers (blue arrow). Bar = 100 μm.

2.2.3. ATR-FTIR spectra changes on skin wound healing induced by AuNP-BP

Results in figure 7 showed the average spectra of WOT, AuNPs, BP and AuNP-BP skin wound healing at 7 days. Main biomolecules characteristics of biological samples are evident, such as lipids, proteins, carbohydrates, and nucleic acids (Figure 7 and Table 2).

The average of skin wound healing with the treatments showed collagen bands, two intense bands at 1660 cm^{-1}, and 1549 cm^{-1}, are related to stretching vibration of C=O functional groups; a combination of C-N stretching and N-H bending vibration in the triple helix of collagens, 1338 cm^{-1} (CH_2 side chain vibrations), 1286 cm^{-1} and 1204 cm^{-1} related to CH_2 wagging vibration from the glycine backbone and proline sidechain and 1082 cm^{-1}, assigned to C-O stretching vibrations of the carbohydrate residue.

The bands at 1737 cm^{-1} (C=O) and, 1456 cm^{-1} (CH_2) are related with lipids, whereas the band at 1400 cm^{-1} arise from CH_3 of GAGs; also phospholipids group absorbs at 1268 cm^{-1} and 1085 cm^{-1}.

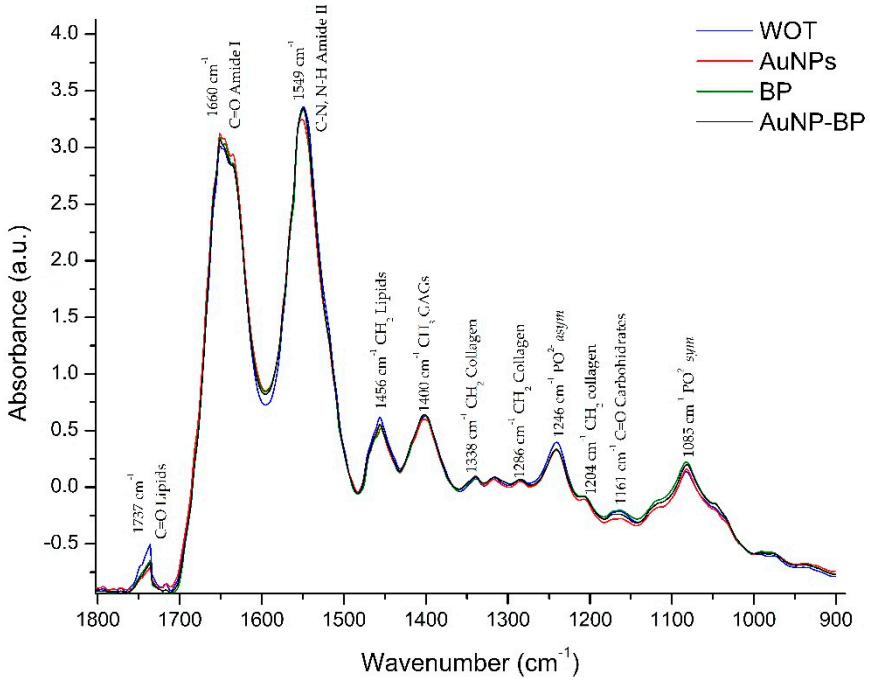

Figure 7. FTIR spectra average of WOT, AuNPs, BP, and AuNP-BP.

Table 2. FTIR bands assigment.

Band		Assignment	Reference
1	1737	C=O lipids	[18]
2	1660	C= O Amide I	[18,19]
3	1549	C-N, N-H Amide II	[18,19]
4	1456	CH_2 lipids	[18,19]
5	1400	CH_3 GAGs	[19]
6	1338	CH_2 Collagen type I	[19]
7	1286	CH_2 collagen Amide III, glycine and proline	[19]
8	1246	PO_2^- *asym* Phospholipds	[18]

Preprints (www.preprints.org) | NOT PEER-REVIEWED | Posted: 23 October 2023 doi:10.20944/preprints202310.1416.v1

9	1204	CH_2 Collagen Amide III	[19]
10	1161	C-O carbohidrates residues	[19]
11	1085	PO_2^- *sym* Phospholipds, C-O of carbohydrate on Collagen and PG	[18,19]

The major peaks with significant shifts are related to Amide I, Amide II, CH_2 lipids, PO_2^- *asym* Phospholipds and PO_2^- *sym* Phospholipds (Figure 8 and Table 3).

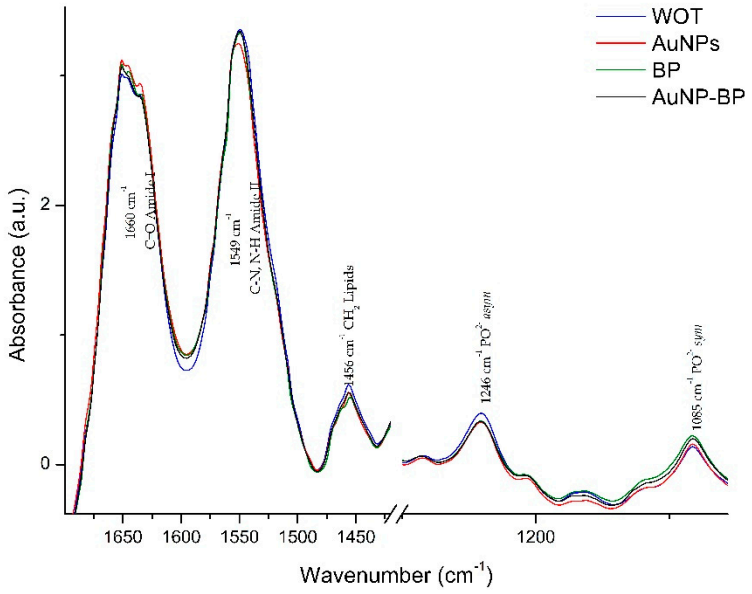

Figure 8. Bands with significant major peak shift. FTIR spectra of skin after 7 days of healing; without treatment (WOT), and with different treatments: AuNPs, BP, and AuNP-BP.

Table 3. FTIR band frequencies observed in skin at 7 day on groups without treatment (WOT), or treated with AuNPs, BP and AuNP-BP.

Band	WOT	AuNPs	BP	AuNP-BP	P
1	1736 (1736, 1736)	1736 (1736, 1736)	1736 (1736, 1736)	1736 (1736, 1736)	0.069
2	1651 (1645, 1651)	1651 (1651, 1651)[a]	1651 (1651, 1651)[a]	1651 (1651, 1651)[a]	0.016
3	1549 (1549, 1549)	1551 (1551, 1552)[a]	1551 (1549, 1551)[a]	1551 (1549, 1551)[ab]	0.000
4	1456 (1454, 1456)	1456 (1456, 1456)	1456 (1454, 1656)[b]	1456 (1456, 1456.)	0.001
5	1402 (1400, 1402)	1402 (1402, 1402)	1402 (1402, 1402)	1402 (1402, 1402)	0.317
6	1339 (1339, 1340)	1339 (1339, 1340)	1339 (1337, 1340)	1340.46 (1339, 1340)	0.713
7	1285 (1283, 1286)	1285 (1285, 1286)	1286 (1285, 1288)	1285 (1285, 1286)	0.081
8	1240 (1240, 1240)	1240 (1240, 1242)	1240 (1240, 1242)	1242 (1240, 1242)[ab]	0.028

Preprints (www.preprints.org) | NOT PEER-REVIEWED | Posted: 23 October 2023 doi:10.20944/preprints202310.1416.v1

9	1207 (1207, 1211)	1207 (1207, 1209)	1209 (1207, 1211)	1209 (1207, 1211)	0.088
10	1163 (1161, 1171)	1164 (1162, 1168)	1163 (1163, 1171)	1167 (1163, 1171)	0.497
11	1082 (1082, 1082)	1082 (1082, 1082)	1082 (1082, 1084)[ab]	1082 (1082, 1082)	0.000

p Kruskal-Wallis test. [a] p <0.05 vs WOT. [b] p <0.05 vs AuNPs.

The absorbances related to Amide II (1549 cm^{-1}), CH_2 lipids and collagen type I (1456 cm^{-1}) and CH_2 collagen (1286 cm^{-1}) decreased in AuNP-BP in comparison with WOT or with AuNPs, while the absorbance of CH_3 GAGs (1400 cm^{-1}), increase between BP and AuNP-BP *vs* AuNPs, bands related to CH_2 collagen (1204 cm^{-1}), C=O carbohydrates (1161 cm^{-1}), and PO_2^- *sym* (1085 cm^{-1}) are increase on BP and AuNP-BP in comparison with AuNPs (Figure 9, table 4).[18–20]

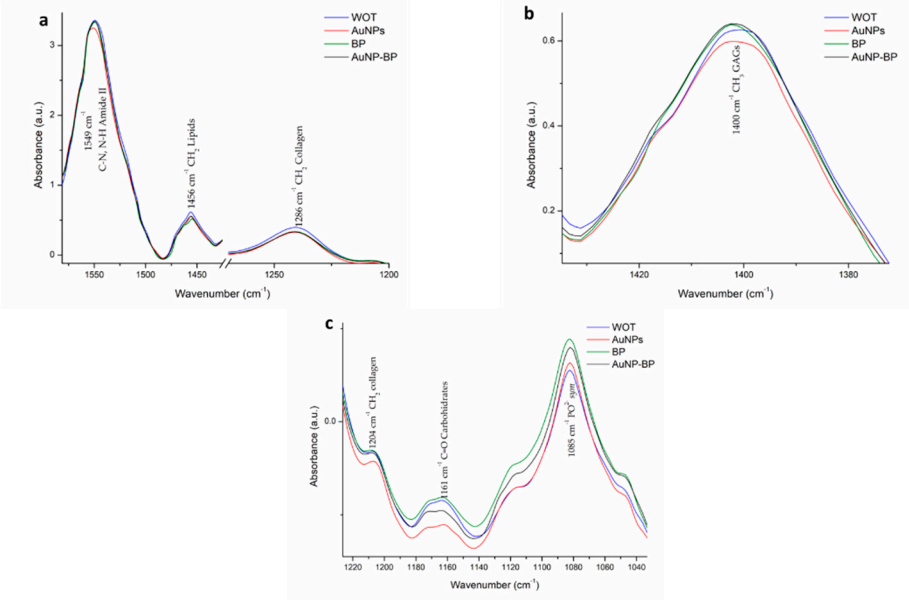

Figure 9. Bands with significant changes on absorbance. a. Bands with significant decrease between BP and AuNP-BP in comparison with WOT or AuNPs. b. bands with an increase in comparison with AuNPs. c. Bands with an increase in comparison with AuNPs.

Table 4. FTIR bands absorbance observed in skin at 7 day on groups without treatment (WOT), treated with gold nanoparticles (AuNPs), BP and conjugate (AuNP-BP).

Band	WOT	AuNPs	BP	AuNP-BP	P
1	0.4 (0.16, 0.64)	0.19(0.12, 0.29)	0.28 (0.23, 0.62)	0.28 (0.23, 0.34)	0.08
2	4.03 (3.88, 4.17)	4.08 (4.96, 4.13)	4.09 (4.06, 4.2)	4.07 (4.03, 4.1)	0.128
3	4.36 (4.33, 4.45)	4.21 (4.19, 4.24)[a]	4.35 (4.24, 4.45)[b]	4.28 (4.24, 4.33)[ab]	0.0001
4	1.58 (1.52, 1.74)	1.51 (1.47, 1.54)	1.55 (1.51, 1.61)[b]	1.53 (1.49, 1.55)[a]	0.012
5	1.64 (1.55, 1.66)	1.56 (1.53, 1.58)[a]	1.63 (1.58, 1.74)[b]	1.63 (1.56, 1.67) [b]	0.001
6	1.06 (1.01, 1.13)	1.06 (1.03, 1.08)	1.09 (1.04, 1.15)	1.06 (1.05, 1.08)	0.305
7	1.06 (1, 1.12)	1.01 (0.98, 1.04)[a]	1.07 (0.99, 1.17) [b]	1.02 (1.02, 1.04)	0.04
8	1.36 (1.28, 1.44)	1.3 (1.23, 1.34)	1.36 (1.25, 1.48)	1.28 (1.26, 1.33)	0.091
9	0.89 (0.84, 0.99)	0.85 (0.81, 0.89)[a]	0.93 (0.84, 1.02) [b]	0.89 (0.86, 0.93) [b]	0.015
10	0.76 (0.72, 0.87)	0.66 (0.63, 0.72)[a]	0.79 (0.69, 0.92) [b]	0.75 (0.69, 0.81) [b]	0.003
11	1.14 (0.99, 1.22)	1.11 (1.07, 1.17)	1.19 (1.13, 1.35)[ab]	1.2 (1.16, 1.23) [b]	0.003

 doi:10.20944/preprints202310.1416.v1

p Kruskal-Wallis test. [a] p <0.05 vs WOT. [b] p <0.05 vs AuNPs.

Results displayed in Figure 10a represents the average of second derivative absorbance related to Amide I, showing the band related to β-sheet at 1665 cm^{-1} and the band related to α-helix at 1660 cm^{-1} [18] We found a significative increase of α-helix/ β-sheet on treatment with AuNP-BP hydrogel in comparison to the other groups of treatments (WOT, AuNPs, and BP) as can be seen in figure 8b.

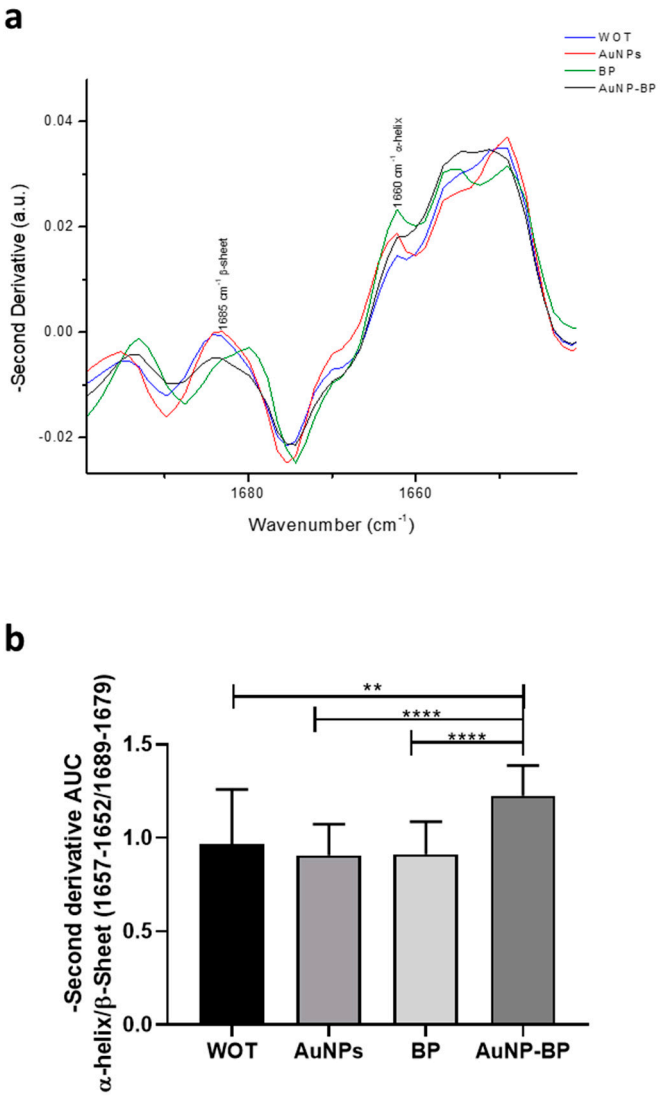

Figure 10. Negative of Second derivative FTIR spectra of Amide I. a. FTIR spectra average of negative second derivative of WOT, AuNPs, BP, and AuNP-BP. b. AUC ratio α-helix/β sheet. ** p <0.01, ****p<0.0001.

3. Discussion

Metallic nanoparticles have gained much attention as powerful materials for nanomedicine, catalysis, environmental research, biosensor, and drug delivery due their physicochemical properties [21].

Gold nanoparticles displayed the surface plasmon resonance phenomenon, responsible of their optical proprieties, permitting to follow and easily control their size, shape and composition [15] . On the other hand, surface modification of AuNPs provide stable matrix for biomolecular functionalization of several molecules such as proteins, organic compounds or plant extracts between

others. Related to plants extracts are uses as capping agents due their phytochemical composition enrichment of flavonoids, phenols and terpenoids, similar to BP [6,21].

Here we conjugated the AuNPs with the bioactive of *B. procumbens* polyphenolic compounds (BP) that promotes tissue repair and wound healing [6]. The characterization of AuNPs synthesis and AuNP-BP conjugation were done by Uv-visible spectrophotometry, FTIR-spectra and DLS and electrophoretic light scattering to determinate their optical properties, size, concentration, agglomeration state, hints on NP shape, surface composition, ligand binding, and hydrodynamic size [10,22].

Conjugation of BP to AuNPs shift the nanoparticles absorbance from 520 nm to 524 nm, the resonance wavelength and band width of AuNPs are dependent on the particle size and shape [15].

The Lambert-Beer law indicates that the absorbance is directly proportional to the extinction coefficient multiplied by the path length and the concentration of the solution. Otherwise, Mie and coworkers, demonstrated that the oscillation modes depend on the particle size and as the size decreases, the maximum absorption also decreases, events that we observed when AuNPs were conjugate with BP [22,23].

Higher concentrations of AuNPs-BP displayed a peak at 668 nm related to the chorophyll α; some reports have shown that higher concentrations of extracts could capping and stabilizing agents such as phenolics, flavonoids, alkaloids, polysaccharides, saponins, tannins, and organic acids, leadding Au-hydro-complex rather than nanoparticles. Thus, we chose the BP concentration of 1.6 mg/ml for the optimum capping formation.[13,21]

According with the FTIIR analyses of BP and AuNPs-BP, peaks at 1700 cm^{-1}, 1610 cm^{-1}, 1512 cm^{-1}, 1450 cm^{-1}, 1375 cm^{-1}, 1258 cm^{-1}, 1230 cm^{-1}, 1171 cm^{-1}, 1076 cm^{-1} and 1045 cm^{-1} suggest that the AuNPs are capping with BP polyphenols previously reported[6], similar to other reports where polyphenols derived from alcoholic extracts natural resources capped gold nanoparticles [16,17].

Nanoparticle size varieties by the instrumentation method due it could change by various interaction forces in solution, including Van der Waals forces. Polyphenols limit particle growth and prevent agglomeration stabilizing the gold nanoparticles [21]. Here we found that gold nanoparticles alone are around 9 nm by UV-Vis spectra, and change to 28 nm when are capping with BP; but when they are measured by DLS, is the initial size measured at 44.51 nm increasing to 44.58 nm, in a similar way as has been describing when the capping is performed [21]. The increment of AuNP-BP sizes measured by the two methods suggest includes the biomolecule compounds, mainly polyphenols, enveloping the core of AuNPs, stabilized the gold nanoparticles.

The zeta potential provides valuable information about the surface charge as well as the stability of AuNPs-BP in colloidal systems [24]. The AuNP-BP potential was -18-2 ± 7.02 mV, indicating an important stabilization; the conjugation of BP compounds increased the AuNPs stability, conferring a higher negative zeta potential. It is known that highly negative zeta potential value indicates that there is enough force to prevent the aggregation of the gold particles, considering value lower than -30 mV as strongly anionic. BP through the functional groups of polyphenols (-OH and –COOH), provide negative charge, like other studies reported [21].

Interestingly, using an hydrogel containing AuNP-BP at 1.6 mg/ml of BP concentration for wound treatment in a wound excision animal model, we showed an enhanced percentage of wound reduction seven days posttreatment in contrast to animals treated with hydrogel containing AuNPs alone. suggesting that the capping compounds derived from BP induced these wound healing effects, as we previous describe with the BP alone [6].

Our findings are in concordance with other reports that showed that gold nanoparticles capping with natural products, such as quercetin derived from *Abelmoschus esculentus* (L.) (okra), enhanced wound healing [25].

BP and AuNP-BP compounds not only showed a better macroscopical effects; it induced a reduction of inflammatory infiltration [25]; increased re-epitelization and better collagen organization, *Abelmoschus esculentus* (L.) (okra), AuNPs showed organized collagen fibers and blood vessels at 12 days [25].

 doi:10.20944/preprints202310.1416.v1

Histological changes suggest that at seven days the lesions are on the proliferative phase, showing the granulation tissue that involves collagen and elastin; collagen also showed better organization when injuries were treated with AuNP-BP as demonstrated by Masson and Picrosiruis Red stainings [26].

By FTIR spectroscopy, we found a shift on collagen bandsamide I and amide II (1651 cm^{-1} and 1549 cm^{-1}), to 1456 cm^{-1}, and 1240 cm^{-1}, respectively. Those shifts suggest conforming changes on helices, that were analyzed by the increase on ratio at 1657 cm^{-1}-1652 cm^{-1}/1689 cm^{-1}-1679 cm^{-1}, which showed an increase in AuNP-BP, demonstrating a better collagen alignment, as it was described by de Campos Vidal and Mello, 2019 [20,27].

Other change observed at 1082 cm^{-1}, is associated to symmetric phosphate stretching from nucleic acids, presented increased in the spectral data on BP and AuNP-BP suggesting an increase on cells proliferation whithin wound enhancing wound healing process[26].

All results together suggest that nanoconjugation of biological compounds could accelerate the wounding healing process diminishing the time of tissue repair having the conformation of tissue with better physiological and mechanical proprieties and diminishing the putative adverse side effects produced by some of the bioactive compounds.

4. Materials and Methods

4.1. Polyphenolic compounds extraction from Bacopa procumbens

We follow the procedure previously described to obtain the aqueous fraction from the B procumbens (Mill.) Greenm to get the polyphenolic compounds [6].

4.2. Gold nanoparticles synthesis

Gold nanoparticles were prepared by chemical reduction of tetrachloroauric acid trihydrate (sigma Aldrich) with sodium citrate dehydrate (Bakker) in water. The AuNPs were synthesized due the citrate ions act as the reducing, and capping agents. This method involved the preparation of 1 ml of HAuCl4 (sigma Aldrich) at 4% in deionized water. A quantity of 0.5 ml of this solution was added to 200 ml of deionized water and brought to boiling with constant stirring. Once the sample reached 97 and 100°C, 3 ml of 1% sodium citrate were added and the solution began to darken and turn bluish gray or purple. After 30 min, the reaction was complete and the final color was a deep wine red indicating that the colloidal dispersion of gold nanoparticles was obtained. After the dispersion was cooled, the AuNPs were centrifuged at 3,500 rpm for 40 min, the supernatant was removed, and the nanoparticles were resuspended in 6 ml of deionized water. The obtained suspension was stored at 4°C [9].

4.3. Gold nanoparticles conjugation with polyphenolic compounds of Bacopa procumbens

Once synthesized, the AuNPs with negative charge provided by the citrate groups located on their surface, were mixed with different concentrations of polyphenolic compounds of *B. procumbens* (BP) to covers the surface of nanoparticles with an BP extract layer. For this purpose, constant volumes of the colloidal dispersion nanoparticles (AuNPs) were mixed with constant volumes of the BP at several concentrations (0.4, 0.8, 1.6, 3.2 and 6.4 mg/mL) overnight, after the conjugate were cleanead by centrifugation twice at 4°C 000 rpm during 10 min. The resulting conjugate nanoparticles (AuNP-BP) were then characterized.

4.4. Instrumentation

Ultraviolet–visible measurements were performed using an Evolution 606 Spectrophotometer (Thermo Scientific). It was used to measure the surface plasmon resonance (SPR) absorption band of single gold nanoparticles (AuNPs), polyphenolic compounds of B. procumbens (BP) and the conjugate (AuNP-BP) [21].

 doi:10.20944/preprints202310.1416.v1

A Fourier transform infrared (FTIR) spectrometer Bruker model Vertex 70 in the attenuated total reflectance (ATR) sampling mode was used to measure the infrared absorptions of AuNPs, BP and AuNP-BP at 1.6 mg/ml. To realize the FTIR measurements, the colloidal samples (AuNPs and AuNP-BP) were centrifuged at 3500 rpm for 40 min; the supernatant was removed and 2 µl of the concentrated sample was placed on the surface of the ATR crystal. The infrared radiation was propagated along the crystal to obtain the corresponding vibrational spectrum, which was averaged from several data acquisitions. The infrared spectra were collected from biological fingprinting 1800 to 800 cm^{-1}.

Zetasizer Nano ZS (Malvern instruments Ldt., Malvern, UK) Dynamic Light Scattering measurements (DLS) and Electrophoretic Ligth Scattering (ELS) techniques were used to analyze the size and the zeta potential of the AuNPs and the AuNP-BP samples after these were diluted with ultrapure distilled water [24].

4.5. In vivo skin wound model

4.5.1. Animals

Sixty male adult Wistar rats (220 –280g) were maintained at 26°C under 12:12 hours light/dark cycle. Animal received chow and water ad libitum and were kept in individual cages. The ethics committee of ENMyH postgraduate section approved the experimental procedure of this study (CBE/010/2019 approval) [6].

The animals were divided into four randomized groups: untreated group (WOT); AuNPs at 5% (AuNPs) into a hydrogel, group treated with polyphenolic compounds of B. procumbens (BP) at 160 mg/ml included into a hydrogel, and AuNP-BP at 1.6 mg/ml into hydrogel. The hydrogel for topical administration was composed by water, carbopol 0.7%, glycerin 1%, hydantoin, methylchloroisothiazolinone, and methylisothiazolinone 0.2% and triethanolamine 1%.

For the excisional wound model, the animals were anesthetized intraperitoneal with ketamine/xilacine (50/5 mg/kg), the dorsal region was harvested and four complete thickness excision surgeries of 1 cm^2 were performed. The wounds were treated daily with 100 µl from the different treatments. Animals were sacrificed at day 7 after injury. Six rats were used for each experimental group [6].

4.5.2. Morphometric analysis

The healings were observed, photographed and measured immediately after surgery (initial wound area) and at day 7 using a Vernier caliper to calculate the percent reduction of wounds as equation (1) [6].

$$\% \text{ of wound reduction} = 100 - [(\text{final area} \times 100)/\text{initial area}] \quad (1)$$

4.5.3. Histopathological analysis

Wound lesions from the different groups at day 7 were surgical removed with adjacent healthy skin, tissues were fixed in 4% buffered paraformaldehyde; embedded in paraffin and sectioned using microtome. Five m thickness sections were stained with hematoxylin & eosin, and PicroSirus-Red reagent (Abcam, Cambridge, UK), according to manufacturer instructions, and then the tissues were observed and photographed using the Olympus DP74 system (Olympus, Tokyo, Japan) and a polarizing light microscope (Nikon, Tokio, Japan). Three different areas from three consecutive sections were analyzed for the descriptive histopathological analysis [6].

4.5.4. ATR-FTIR spectra analysis

The biomolecular and structural analysis of wounds were done through vibrational spectroscopy, the samples were put directly on the surface of the ATR crystal, for the acquisition of their FTIR spectra; WOT, AuNPs, BP and AuNP-BP were analyzed by FTIR as describe before in instrumentation section.

Spectral analysis was performed on the fingprint region (1800-800 cm -1) using the OPUS software, absorbance spectra were normalized using a standard normal variate (SNV) normalization employing the Unscrambler X software (version 10.3, Camo). The bands related to lipids, proteins, collagen and phosphates were identified in each spectrum and the average spectra were calculated.

The frequencies of the bands and absorbances of the spectra were analyzed by using the Origin software (version 6.1, Origin Lab Corporation). Then, the second derivative was calculated employing the Savitzky-Golay algorithm with five points windows for smothing and the second polynomial order using the Unscrambler X. The second derivative is a mathematical tool that allows observe absorption bands related with the secondary structure of proteins. In this case, the secondary structure (α-helix and β-sheet) related with several types of collagen, in the Amide I region (1700-1600 cm^{-1}) were observed [18].

The integrate area corresponding to α-helix (1657-1652 cm^{-1}) and β-sheet (1689-1679 cm^{-1}) on the second derivative were obtained in order to calculate de ratio of α -helix/β-sheet [20].

4.6. Statistical analysis

Statistical significance was analyzed using ANOVA post hoc Turkey´s test or Kruskal- Wallis according at data distribution. All analyses were performed using Graph Pad Prism software version 7.0.

5. Conclusions

The results suggest that polyphenolic compounds from bacopa procumbens are capping gold nanoparticles, enhancing the effect of BP alone reducing the concentration 100 folds, and enhancing the skin wound healing on the proliferative phase, improving collagen organization by histological and FTIR findings, reducing the inflammatory process and reflecting in macroscopical effect.

6. Patents

Patent derived from this paper and previous work (poner la referencia) is patentwith number 376170.

Author Contributions: Conceptualization, D.G.P.-I. and M.d.C.G.-G; methodology, A.M.-C. M.M.M-M; software, M.R.L.; validation, M.R.L., J.O.L. and R.J.D.M.; formal analysis, A.M.-C., D.G.P.-I.; M.R.L; G.J.V-Z.; investigation, A.M.-C. and M.R.L.; resources, D.G.P.-I. and M.d.C.G.-G.; writing—original draft preparation. A.M.-C. and D.G.P.-I.; writing—review and editing, A.M.-C., D.G.P.-I and M.R.L.; visualization, D.G.P.-I. and M.R.L..; supervision, D.G.P.-I., M.d.C.G.-G.; M.R.L. and R.J.D.M project administration, D.G.P.-I. and M.d.C.G.-G.; funding acquisition, D.G.P.-I. and M.d.C.G.-G. All authors have read and agreed to the published version of the manuscript.

Funding: This research was funded by: 20131895, 20140196, 20150289 SIP-IPN and 20174892, 20172333 innovation-IPN given to D.G.P.-I.; and 20131836, 20140313 and 20150308 SIP-IPN given to M.d.C.G.-G.

Institutional Review Board Statement: The ethics committee of the ENMyH postgraduate section approved the experimental procedure of this study (approval number CBE009/2019).

Informed Consent Statement: Not applicable

Data Availability Statement: The data that support the findings of this study are available on request from the corresponding author.

Acknowledgments: We would like to acknowledge José Pérez González of ESFM for the use of the Nikon Eclipse LV100 microscope.

Conflicts of Interest: The authors declare no conflict of interest

References

1. Kwan KH, Liu X, To MK, Yeung KW, Ho CM, Wong KK. Modulation of collagen alignment by silver nanoparticles results in better mechanical properties in wound healing. Nanomedicine. **2011**, 7(4):497-504. doi: 10.1016/j.nano.2011.01.003.

2. Velnar T, Bailey T, Smrkolj V. The wound healing process: an overview of the cellular and molecular mechanisms. J Int Med Res. **2009**, 37(5):1528-42. doi: 10.1177/147323000903700531.
3. Spampinato SF, Caruso GI, De Pasquale R, Sortino MA, Merlo S. The Treatment of Impaired Wound Healing in Diabetes: Looking among Old Drugs. Pharmaceuticals (Basel). **2020**, 13(4):60. doi: 10.3390/ph13040060.
4. Naskar A, Kim KS. Recent Advances in Nanomaterial-Based Wound-Healing Therapeutics. Pharmaceutics. **2020**, 12(6):499. doi: 10.3390/pharmaceutics12060499.
5. Melguizo-Rodríguez L, de Luna-Bertos E, Ramos-Torrecillas J, Illescas-Montesa R, Costela-Ruiz VJ, García-Martínez O. Potential Effects of Phenolic Compounds That Can Be Found in Olive Oil on Wound Healing. Foods. **2021**, 10(7):1642. doi: 10.3390/foods10071642.
6. Martínez-Cuazitl A, Gómez-García MDC, Hidalgo-Alegria O, Flores OM, Núñez-Gastélum JA, Martínez ESM, Ríos-Cortés AM, Garcia-Solis M, Pérez-Ishiwara DG. Characterization of Polyphenolic Compounds from Bacopa procumbens and Their Effects on Wound-Healing Process. Molecules. **2022**, 27(19):6521. doi: 10.3390/molecules27196521.
7. Cucci LM, Trapani G, Hansson Ö, La Mendola D, Satriano C. Gold Nanoparticles Functionalized with Angiogenin for Wound Care Application. Nanomaterials (Basel). **2021**, 11(1):201. doi: 10.3390/nano11010201.
8. Grzelczak M, Pérez-Juste J, Mulvaney P, Liz-Marzán LM. Shape control in gold nanoparticle synthesis. Chem Soc Rev. **2008**, 37(9):1783-91. doi: 10.1039/b711490g.
9. Wang A, Ng HP, Xu Y, Li Y, Zheng Y, Yu J, et al. Gold nanoparticles: Synthesis, stability test, and application for the rice growth. J Nanomater. **2014**, 2014:3–6. doi: 10.1155/2014/451232
10. Mourdikoudis S, Pallares RM , Thanh NTK . Characterization techniques for nanoparticles: comparison and complementarity upon studying nanoparticle properties. Nanoscale. **2018**, 10(27):12871-12934. doi: 10.1039/c8nr02278j.
11. Kus-Liśkiewicz M, Fickers P, Ben Tahar I. Biocompatibility and Cytotoxicity of Gold Nanoparticles: Recent Advances in Methodologies and Regulations. Int J Mol Sci. **2021**, 22(20):10952. doi: 10.3390/ijms222010952.
12. Rua J. Kadhim, Esraa H. Karsh, Zainab J. Taqi, Majid S. Jabir, Biocompatibility of gold nanoparticles: In-vitro and In-vivo study, Materials Today: Proceedings. **2021,** 42(5):3041-3045, ISSN 2214-7853, https://doi.org/10.1016/j.matpr.2020.12.826.
13. Sandiningtyas RD, Suendo V. Isolation of chlorophyll from spinach and its modification using Fe2+ in photostability study. In: Third international conference on mathematics and natural science. **2010**, pp 859–873
14. Aravinthan A, Kamala-Kannan S, Govarthanan M, Kim JH. Accumulation of biosynthesized gold nanoparticles and its impact on various organs of Sprague Dawley rats: a systematic study. Toxicol Res (Camb). **2016**, 5(6):1530-1538. doi: 10.1039/c6tx00202a.
15. Ha Lien, Nghiem Thi & La, Huyen & Xuan Hoa, Vu & Chu, Viet Ha & Nguyen, Thanh & Fort, Emmanuel & Do Quang, Hoa & Hong Nhung, Tran. Synthesis, capping and binding of colloidal Gold Nanoparticles to Proteins. Advances in Natural Sciences: Nanoscience and Nanotechnology. **2010**, 1. 025009. 10.1088/2043-6254/1/2/025009.
16. Sanna V, Pala N, Dessì G, Manconi P, Mariani A, Dedola S, Rassu M, Crosio C, Iaccarino C, Sechi M. Single-step green synthesis and characterization of gold-conjugated polyphenol nanoparticles with antioxidant and biological activities. Int J Nanomedicine. **2014**, 9:4935-51. doi: 10.2147/IJN.S70648.
17. Oliveira RN, Mancini MC, Oliveira FCS de, Passos TM, Quilty B, Thiré RM da SM, et al. FTIR analysis and quantification of phenols and flavonoids of five commercially available plants extracts used in wound healing. Matéria (Rio J) [Internet]. **2016**, 21(3):767–79 https://doi.org/10.1590/S1517-707620160003.0072
18. Vazquez-Zapien GJ, Martinez-Cuazitl A, Granados-Jimenez A, Sanchez-Brito M, Guerrero-Ruiz M, Camacho-Ibarra A, Miranda-Ruiz MA, Dox-Aguillón IS, Ramirez-Torres JA, Mata-Miranda MM. Skin wound healing improvement in diabetic mice through FTIR microspectroscopy after implanting pluripotent stem cells. APL Bioeng. **2023**, 7(1):016109. doi: 10.1063/5.0130383.
19. Sanden KW, Kohler A, Afseth NK, Böcker U, Rønning SB, Liland KH, Pedersen ME. The use of Fourier-transform infrared spectroscopy to characterize connective tissue components in skeletal muscle of Atlantic cod (Gadus morhua L.). J Biophotonics. **2019**, 12(9):e201800436. doi: 10.1002/jbio.201800436.
20. Nguyen TT, Eklouh-Molinier C, Sebiskveradze D, Feru J, Terryn C, Manfait M, Brassart-Pasco S, Piot O. Changes of skin collagen orientation associated with chronological aging as probed by polarized-FTIR micro-imaging. Analyst. **2014**, 139(10):2482-8. doi: 10.1039/c3an00353a.
21. Aji A, Oktafiani D, Yuniarto A, Kurnia AA, Biosynthesis of gold nanoparticles using Kapok (Ceiba pentandra) leaf aqueous extract and investigating their antioxidant activity, Journal of Molecular Structure. **2022**, 1270:133906, https://doi.org/10.1016/j.molstruc.2022.133906.
22. González, V., Kharisov, B. & Gómez, I. Preparation, optical characterization and stability of gold nanoparticles by facile methods. Revista Mexicana de Fisica. **2019**, 65: 690–698.

23. Haiss W, Thanh NT, Aveyard J, Fernig DG. Determination of size and concentration of gold nanoparticles from UV-vis spectra. Anal Chem. **2007**, 79(11):4215-21. doi: 10.1021/ac0702084.
24. Elbagory AM, Hussein AA, Meyer M. The In Vitro Immunomodulatory Effects Of Gold Nanoparticles Synthesized From Hypoxis hemerocallidea Aqueous Extract And Hypoxoside On Macrophage And Natural Killer Cells. Int J Nanomedicine. **2019**, 14:9007-9018. doi: 10.2147/IJN.S216972.
25. Korani S, Rashidi K, Hamelian M, Jalalvand AR, Tajehmiri A, Korani M, Sathyapalan T, Sahebkar A. Evaluation of Antimicrobial and Wound Healing Effects of Gold Nanoparticles Containing Abelmoschus esculentus (L.) Aqueous Extract. Bioinorg Chem Appl. **2021**, 2021:7019130. doi: 10.1155/2021/7019130.
26. Castro PAA, Lima CA, Morais MRPT, Zorn TMT, Zezell DM. Monitoring the Progress and Healing Status of Burn Wounds Using Infrared Spectroscopy. Appl Spectrosc. **2020**, 74(7):758-766. doi: 10.1177/0003702820919446.
27. Vidal Bde C, Mello ML. Collagen type I amide I band infrared spectroscopy. Micron. **2011,** 42(3):283-9. doi: 10.1016/j.micron.2010.09.010.